Supplementary Materials

Experimental details

Synthesis

All the materials needed for the synthesis of, $[C_3N_2H_5]_3Bi_2I_9$ (**PBI**) and $[C_3N_2H_5]_3Sb_2I_9$ (**PSI**) were purchased from commercial sources (Sigma-Aldrich and Merck (HI)) and used without further purification: $[C_3N_2H_5]I$ (>98%), SbI3(>99,998%), BiI3(>99,998%), HI (57%). The crystals were grown by a slow evaporation of a concentrated HI solution containing the 3:2 ratio of $[C_3N_2H_5]I$ and SbI_3 or BiI_3. The salts obtained were twice recrystallized from a methanol solution and their composition was verified by an elemental analysis: **PBI** C: 6.2% (theor. 6.12%), N: 4.8% (theor 4.76%), H: 0.9% (theor. 0.86%) and **PSI** C: 6.7% (theor. 6.79%), N: 5.2% (theor 5.28%), H: 0.9% (theor. 0.95%). The single crystals suitable for X-ray measurements were grown from an aqueous solution at a constant room temperature.

Thermal analysis

Differential scanning calorimetry (DSC) heating traces were obtained using a Mettler Toledo DSC 3 differential scanning calorimeter calibrated using n-octane and indium. Hermetically sealed Al pans with the polycrystalline material were prepared in an air atmosphere. The measurements were performed between 100 and 400 K. Simultaneous thermogravimetric analysis (TGA) and Differential scanning calorimetry (DSC) were carried out on a Mettler Toledo TGA/DSC 3+ instruments in the temperature range 300-600 K with a ramp rate 5 $K\cdot min^{-1}$ in the nitrogen atmosphere (flow rate: 1 $dm^3\cdot h^{-1}$).

X-ray diffraction

Single-crystal x-ray diffraction was carried out with Mo*Kα* radiation using a Xcalibur, Atlas diffractometer. Diffraction data were processed by *CrysAlis PRO* 1.171.38.43 [1] (Rigaku Oxford Diffraction, 2015). Multi-scan empirical absorption correction using spherical harmonics, implemented in SCALE3 ABSPACK scaling algorithm was applied. The structures were solved and refined using SHELXS and SHELXL2018/3 [2]. H-atom parameters were constrained. Phase **II** in both $PyrBi_2I_9$ and $PyrSb_2I_9$ was refined in orthorhombic *Cmcm* space group at 280 and 285K, respectively. In both crystals, after the low-temperature phase transition the diffraction image was characteristic of a twinned sample indicating a reduction of the crystal class. Low-temperature Phase **II** of **PBI** was refined basing on two twin components in $P2_1/n$ at 100K. In the case of **PSI** the complex twinning with very tinny ferroelastic domains did not allow for a satisfactory refinement of the low-temperature Phase **III**. **PBI** Phase **II (280K)**: a=8.7327(6) Å, b=17.1518 (10)Å, c=22.4125(12) Å; V=3357.0(4) $Å^3$, R(F2 > 2σ(F2)) =0.064, wR(F2)= 0.216, S=1.25; Phase **III (100K):** a= 9.874 (2) Å, b=14.249 (3) Å, c=22.430 (4) Å, 3155.7 (10) $Å^3$, R(F2 > 2σ(F2)) =0.074, wR(F2)= 0.181, S=0.78. **PSI** Phase **II (285K):** a=8.7193 (6) Å, b=17.2789 (10) Å, c=22.2537 (12) Å; V=3352.7 (4) $Å^3$, R(F2 > 2σ(F2)) =0.078, wR(F2)= 0.251, S=1.02. The crystal data, data collection and refinement results are shown in Table S1 in ESI. Selected distances and angles are given in Table S2, whereas hydrogen bond geometry in Table S3. The structures have been deposited in CCDC with deposition numbers: 2105339-2105341.

Dielectric properties

The complex dielectric permittivity, $\varepsilon^* = \varepsilon' - i\varepsilon''$, measurements were conducted on **PBI** and **PSI** in a form of polycrystalline pellets on an Agilent E4980A Precision LCR Meter between 100 and 400 K in the frequency range between 900 Hz and 2 MHz. The gold electrodes were sputtered on both opposite sides of the pellets. The overall errors of ε′ and ε″ were less than 5%. The diameter of the pellet was of the order of 5 mm and its thickness – 1 mm.

UV-Vis spectra

Absorption spectra of crystals, grounded in mortar and suspended in Nujol and placed between two quartz plates, were recorded using a Cary 5000 UV/Vis/NIR at room temperature. The spectra were corrected by subtracting the absorption spectrum of Nujol. The band structure and projected density of states were calculated with the Wien 2k package [3] using the PBE-GGA functional [4]. All calculations were carried out using experimental, not optimized structure and mean atomic positions to remove disorder. The muffin-tin radii (RMTs) were set to 2.5 for Bi, Sb, I; 1.12 for C; 1.04 for N; 0.56 for H. RKmax parameter was set to 8.0. K-paths for band structure calculations [5] were prepared in XCrysDen [6] and consisted of 160 (100 K) or 140 k-points (280 K). Spin-orbit coupling was taken into account in all calculations.

Polarized Light Microscopy

The optical observations were carried out in the polarized light by means of the Olympus BX53 microscope in the temperature range between 100 and 400 K. The temperature was stabilized using the Linkam HTNS 600 heating and freezing microscope stage with a LNP cooling system. The microphotographs were taken using the Olympus BXC50 camera. The temperature rate was equal to 2 K/min.

Solid state NMR

The NMR measurements were made using an ELLAB TEL-Atomic PS 15 spectrometer. Spin–lattice relaxation times, T_1, at 25 MHz were measured using a saturation sequence of $\pi/2$ pulses followed by a variable time interval τ and a reading $\pi/2$ pulse. The magnetization was found to recover exponentially within experimental error at all temperatures. The temperature of the sample was controlled by a UNIPAN 660 temperature controller operating on Pt100 sensor providing long time temperature stability better than 1 K. The samples of powdered GBI and GSI were degassed at room temperature and then sealed under vacuum in a glass ampoule. All measurements were made on heating the sample from liquid nitrogen temperature. The error in the measurements of T_1 was estimated to be about 5%.

Structural results

Table S1. Experimental details

	PBI, Phase II	**PBI, Phase III**	**PSI, Phase II**
Crystal data			
Chemical formula	$C_9H_{15}Bi_2I_9N_6$	$C_9H_{15}Bi_2I_9N_6$	$C_9H_{15}Sb_2I_9N_6$
M_r	1767.33	1767.33	1592.87
Crystal system, space group	Orthorhombic, *Cmcm*	Monoclinic, $P2_1/n$	Orthorhombic, *Cmcm*
Temperature (K)	280	100	285
a, b, c (Å)	8.7327 (6), 17.1518 (10), 22.4125 (12)	9.874 (2), 14.249 (3), 22.430 (4)	8.7193 (6), 17.2789 (10), 22.2537 (12)
α, β, γ (°)	90, 90, 90	90, 90.211 (15), 90	90, 90, 90
V (Å^3)	3357.0 (4)	3155.7 (10)	3352.7 (4)
Z	4	4	4
μ (mm^{-1})	18.76	19.95	9.91
Crystal size (mm)	0.17 × 0.12 × 0.05	0.21 × 0.15 × 0.05	0.15 × 0.13 × 0.02
Data collection			
T_{min}, T_{max}	0.098, 1.000	0.596, 1.000	0.160, 1.000
No. of measured, independent and	9694, 1750, 1166	17109, 17109, 5314	8952, 1741, 1127

observed [$I > 2\sigma(I)$] reflections			
R_{int}	0.054	two-component twin	0.059
$(\sin \theta/\lambda)_{max}$ (Å^{-1})	0.610	0.625	0.610
Refinement			
$R[F^2 > 2\sigma(F^2)]$, $wR(F^2)$, S	0.064, 0.216, 1.25	0.074, 0.181, 0.78	0.078, 0.251, 1.02
No. of reflections	1750	17109	1741
No. of parameters	55	164	40
No. of restraints	22	90	22
$\Delta\rangle_{max}$, $\Delta\rangle_{min}$ (e Å^{-3})	1.12, -1.59	3.08, -2.18	1.15, -1.48

Table S2. Selected geometric parameters (Å, º)

PBI Phase I			
Bi1—I3	2.9755 (14)	Bi1—I2	3.2295 (19)
Bi1—I3^{i}	2.9755 (13)	Bi1—I4	3.2364 (13)
Bi1—I5	2.977 (2)	Bi1—I4^{ii}	3.2364 (13)
I3—Bi1—I3^{i}	93.07 (6)	I2—Bi1—I4	81.48 (4)
I3—Bi1—I5	93.22 (4)	I3—Bi1—I4^{ii}	172.47 (4)
I3^{i}—Bi1—I5	93.22 (4)	I3^{i}—Bi1—I4^{ii}	92.00 (4)
I3—Bi1—I2	92.72 (4)	I5—Bi1—I4^{ii}	92.05 (4)
I3^{i}—Bi1—I2	92.72 (4)	I2—Bi1—I4^{ii}	81.48 (4)
I5—Bi1—I2	171.37 (6)	I4—Bi1—I4^{ii}	82.43 (5)
I3—Bi1—I4	92.00 (4)	Bi1^{iii}—I2—Bi1	81.91 (6)
I3^{i}—Bi1—I4	172.47 (4)	Bi1^{iii}—I4—Bi1	81.70 (4)
I5—Bi1—I4	92.05 (4)		
PBI Phase II			
Bi1—I7	2.968 (3)	Bi2—I6	2.965 (3)
Bi1—I8	2.972 (3)	Bi2—I5	2.984 (3)
Bi1—I9	3.002 (3)	Bi2—I4	2.995 (3)
Bi1—I1	3.184 (3)	Bi2—I1	3.177 (3)
Bi1—I3	3.189 (3)	Bi2—I3	3.192 (3)
Bi1—I2	3.242 (3)	Bi2—I2	3.240 (3)

I7—Bi1—I8	90.98 (9)	I5—Bi2—I4	91.71 (9)
I7—Bi1—I9	93.82 (9)	I6—Bi2—I1	91.92 (9)
I8—Bi1—I9	91.75 (9)	I5—Bi2—I1	95.16 (9)
I7—Bi1—I1	91.98 (9)	I4—Bi2—I1	170.82 (10)
I8—Bi1—I1	95.18 (9)	I6—Bi2—I3	174.41 (11)
I9—Bi1—I1	170.88 (10)	I5—Bi2—I3	93.52 (9)
I7—Bi1—I3	174.41 (11)	I4—Bi2—I3	89.21 (9)
I8—Bi1—I3	93.47 (9)	I1—Bi2—I3	84.32 (9)
I9—Bi1—I3	89.43 (9)	I6—Bi2—I2	94.28 (9)
I1—Bi1—I3	84.25 (9)	I5—Bi2—I2	173.21 (10)
I7—Bi1—I2	94.27 (9)	I4—Bi2—I2	92.26 (9)
I8—Bi1—I2	173.11 (10)	I1—Bi2—I2	80.33 (8)
I9—Bi1—I2	92.35 (9)	I3—Bi2—I2	81.03 (8)
I1—Bi1—I2	80.19 (8)	Bi2—I1—Bi1	82.33 (7)
I3—Bi1—I2	81.04 (8)	Bi2—I2—Bi1	80.48 (7)
I6—Bi2—I5	90.93 (9)	Bi1—I3—Bi2	82.02 (7)
I6—Bi2—I4	94.04 (9)		
PSI Phase I			
SB1—I3	2.9107 (18)	SB1—I2	3.210 (3)
SB1—I3i	2.9107 (18)	SB1—I4ii	3.2119 (19)
SB1—I5	2.912 (3)	SB1—I4	3.2119 (19)
I3—SB1—I3^{i}	93.11 (8)	I2—SB1—I4^{ii}	81.75 (5)
I3—SB1—I5	92.96 (6)	I3—SB1—I4	91.67 (5)
I3^{i}—SB1—I5	92.96 (6)	I3^{i}—SB1—I4	172.77 (7)
I3—SB1—I2	92.60 (5)	I5—SB1—I4	92.21 (6)
I3^{i}—SB1—I2	92.60 (5)	I2—SB1—I4	81.75 (5)
I5—SB1—I2	171.91 (8)	I4^{ii}—SB1—I4	83.08 (7)
I3—SB1—I4^{ii}	172.77 (7)	SB1—I2—SB1^{iii}	81.28 (8)
I3^{i}—SB1—I4^{ii}	91.67 (5)	SB1—I4—SB1^{iii}	81.22 (7)
I5—SB1—I4^{ii}	92.21 (6)		

Symmetry code(s): (i) -*x*, *y*, *z*; (ii) -*x*, *y*, -*z*+1/2; (iii) *x*, *y*, -*z*+1/2.

Table S3. Selected hydrogen-bond parameters in PBI Phase II

D—H···*A*	*D*—H (Å)	H···*A* (Å)	*D*···*A* (Å)	*D*—H···*A* (°)
PhaseII				
N1—H1···I9	0.86	2.67	3.48 (4)	157.4
N2—H2···I8	0.86	2.97	3.73 (4)	147.8
N6—H6···I5	0.86	2.85	3.65 (4)	154.5
N7—H7···I4	0.86	2.73	3.51 (4)	151.9

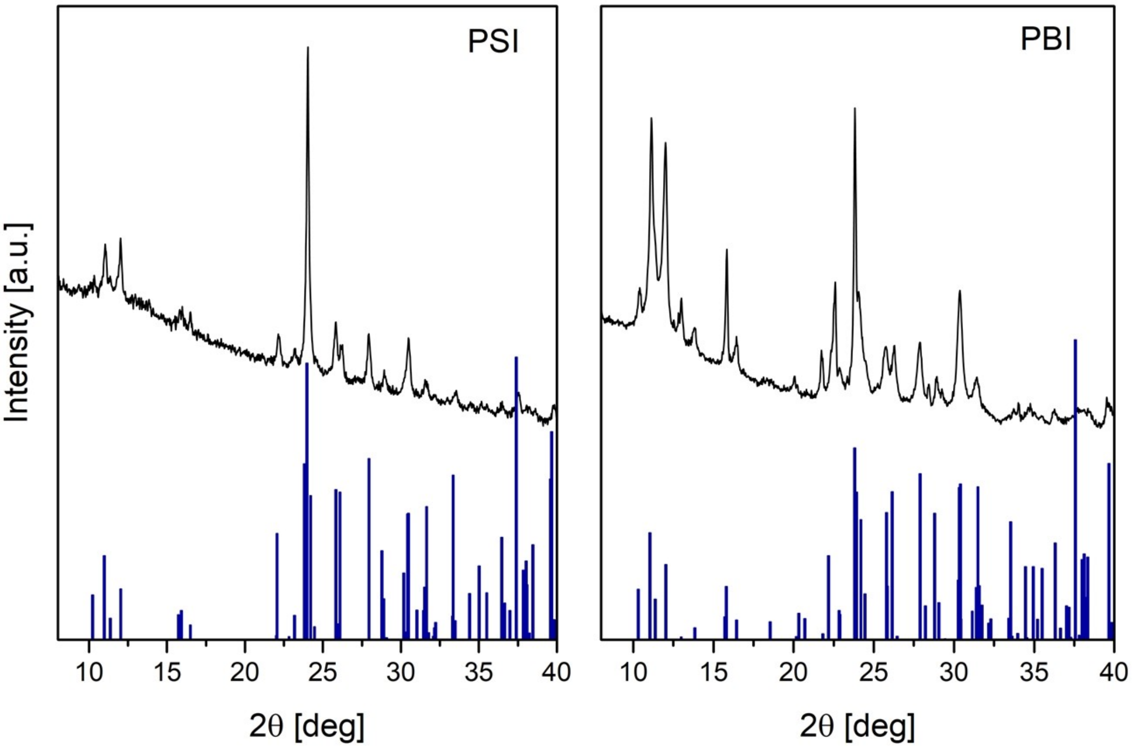

Fig S1. Powder diffraction data for **PSI** (left) and **PBI** (right) measured at room temperature. The positions of the Bragg peaks (marked at the bottom of the graphs) were generated from models of the structure determined at 280 K for **PBI** and 285 K for **PSI**, thus, negligible shifts of the patterns may be expected due to the slightly different lattice parameters. The diffracted intensities are significantly disturbed by the preferred orientation, as the crystallites of both compounds are highly anisotropic.

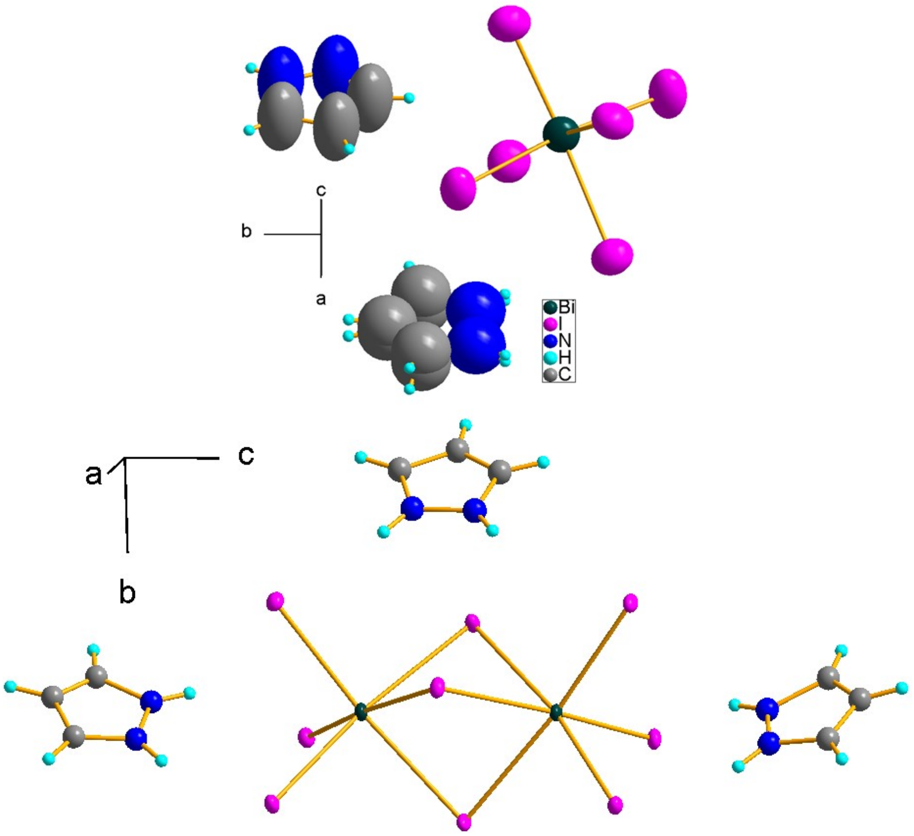

Fig S2. The ellipsoid representation at the 30% probability level of the basic building units in phase II (top) and III (bottom) in $(Pyr)_3M_2I_9$ analogue.

Thermal analysis

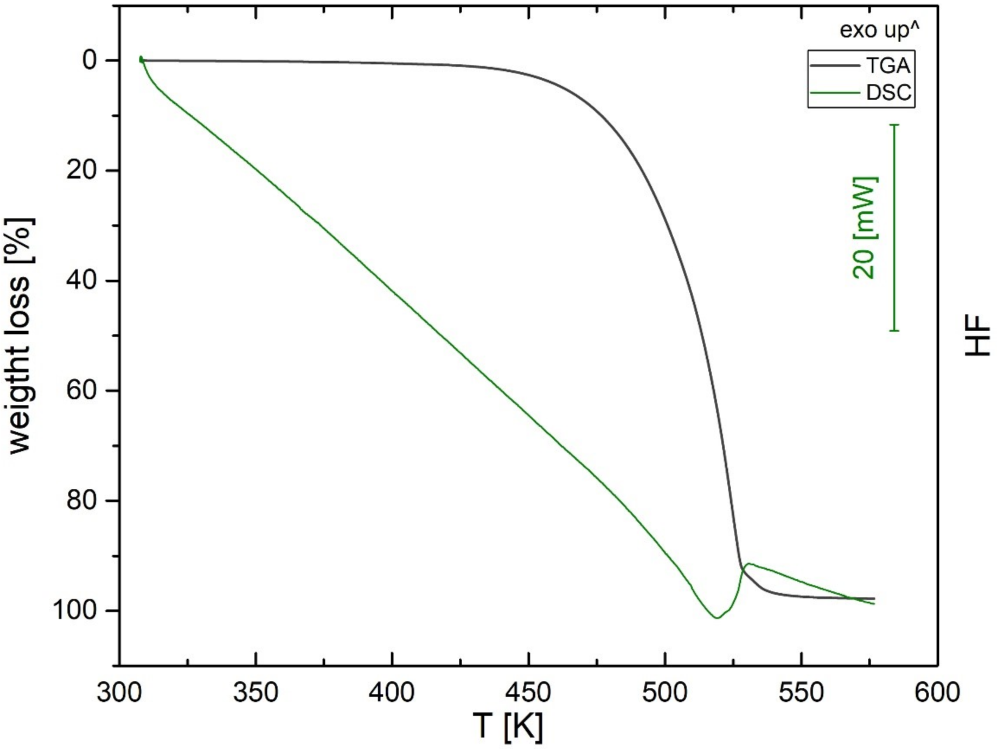

Fig. S3. The TGA and DSC signals for **PSI**.

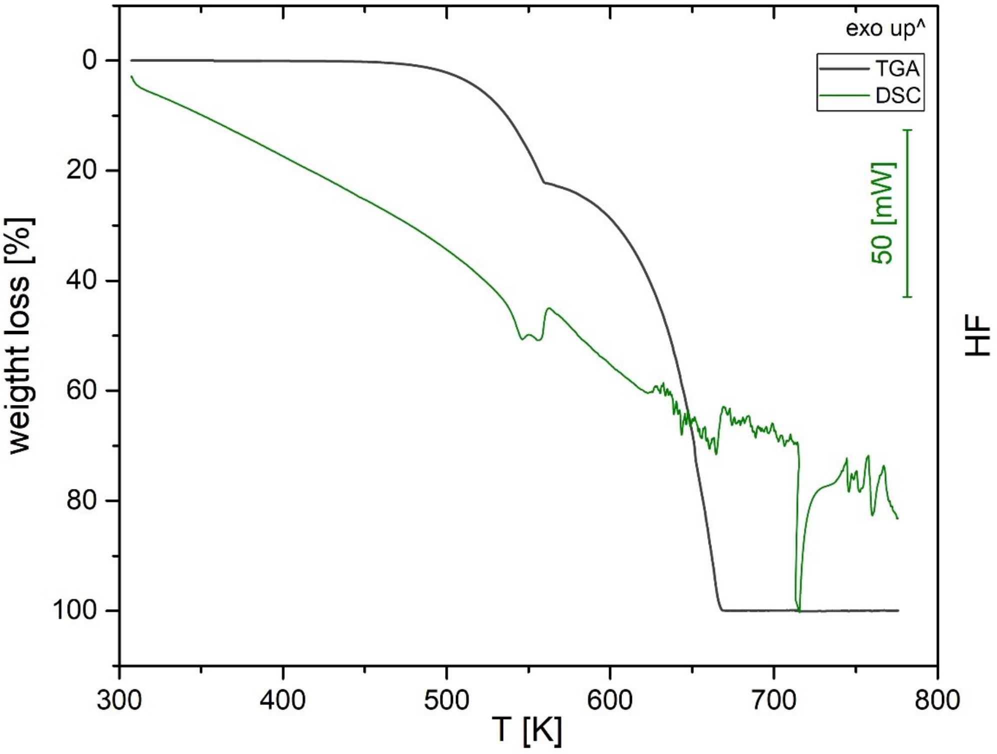

Fig. S4. The TGA and DSC signals for **PBI**.

Table S4. Thermodynamic parameters of the phase transition for **PSI** and **PBI** in the solid state.

Parameters	**$(C_3N_2H_5)_3Sb_2I_9$**	**$(C_3N_2H_5)_3Bi_2I_9$**
M [g·mol^{-1}]	1592.9	1767.4
T_{onset} [K] (coling/heating)		
I→II	366.8/366.3	
II→III	274.6/275.5	370.8/365.2
III→IV	233.3/233.3	252.6/257.9
IV→V	142.8/143.1	
ΔS [J·mol $^{-1}$·K^{-1}] (coling/heating)		
I→II	0.1/0.7	
II→III	12.5/11.4	0.7/0.1
III→IV	-/-	20.0/19.0
IV→V	19.9/18.6	

The T_1 and M_2 measurements

Table S5. The 1H NMR relaxation parameters

temperature range	parameter	PBI	PBI
	E_{a1} [kJ/mol	7.23	7.44
	τ_{01} [s]	$2.84\ 10^{-13}$	$5.3\ 10^{-13}$
	C_1 [s^{-2}]	$4.95\ 10^{8}$(15MHz)	$5.04\ 10^{8}$
	E_{a2} [kJ/mol]	25.59	-
	τ_{02} [s]	$2.56\ 10^{-15}$	-
	C_2 [s^{-2}]	$2.14\ 10^{8}$	-
155K ÷ 220K	E_a [kJ/mol		9.88
233K ÷ 274.6K	E_a [kJ/mol		32.7
>366.6K	E_a [kJ/mol		7.55
>370.8K	E_a [kJ/mol	21.3	

The second-moment values, M_2, for protons in the **PBI** sampleshow that between 170 and 260 K the value of M_2 is continuously reduced from about 4 G^2 to about 1 G^2 in a form of one distinct reduction. Such a simple reduction allows us to analyze the observed temperature dependence of the second moment of ^{1}H NMR line with the BPP formula [7]:

$$M_2 = M_2^{\mathrm{Motion}} + (\, M_2^{\mathrm{Rigid}} - M_2^{\mathrm{Motion}})\tfrac{2}{\pi}\tan^{-1}(\gamma_H \tau_c \sqrt{M_2}), \qquad (1)$$

where $\tau_c = \tau_0 \exp(E_a/RT)$, $M^{\mathrm{Rigid}}{}_2$ and $M^{\mathrm{Motion}}{}_2$ are the second-moment values before and after the onset of a given motion, respectively. The obtained fitting parameters are collected in Table S5. Such a temperature dependence of M_2 results from the process of activation of pseudo C_5 jumps around the axis perpendicular to the cation plane and passing through its center.

This time it should be noted that the experimentally measured value of the second moment, M_2, corresponds perfectly to the value calculated from the well-known van Vleck formula[8] using only crystallographic data. The rigid value of M_2 calculated from the crystal structure determined at 100 K for **PBI** appeared to be about $M_2^{intra} = 2.65\ G^2$ with assumed lengths of bonds for hydrogen's: C-H 1.09 Å and N-H 1.03 Å. The value for total M_2^{rigid} should be supplemented by a part related to the interactions between cations of approximately $M_2^{inter} \sim 1\ G^2$. The value of total M_2^{rigid} determined from theoretical calculations is in perfect agreement with the value determined from the experiment. Note that both visible reductions of M_2 appear at temperatures much lower than the phase transition temperatures, meaning that both 252 K and 370 K phase transitions are related to the molecular dynamic changes of anions. Small reduction of the second moment ($\sim\Delta M_2 = 0.5\ G^2$) observed around 345 K may be related to the possible appearance of a proton conductivity mechanism, the effect of which requires further analysis.

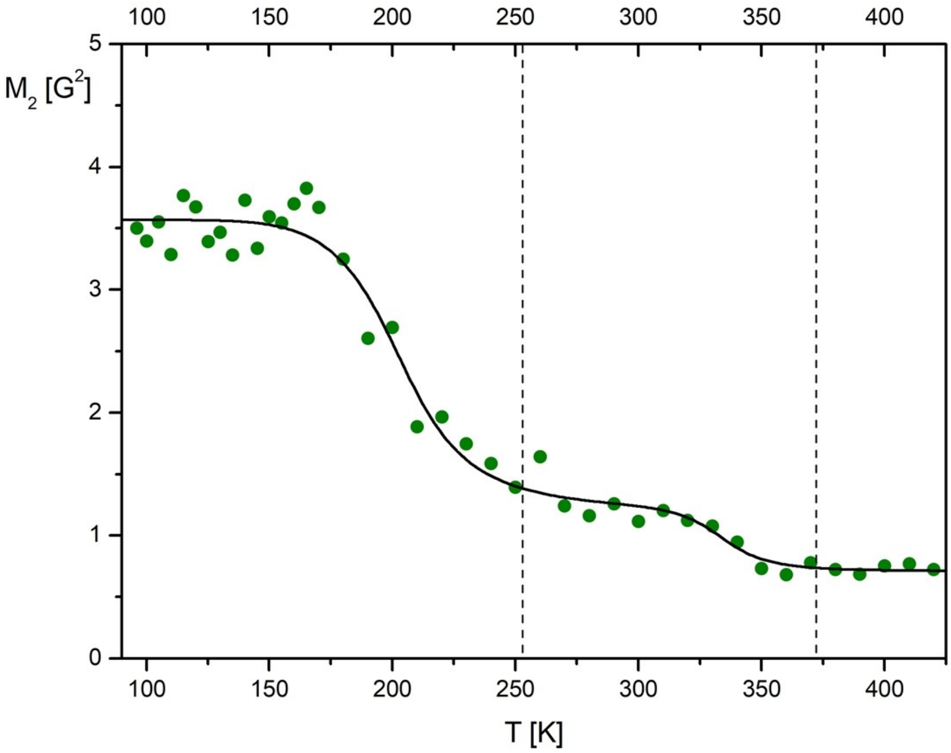

Fig. S5. Temperature dependence of the second moment M_2 of **PBI** for the ^1H NMR line. The solid line was calculated by using the best-fit parameters given in Table S6.

Table S6. The van Vleck parameters of M_2.

parameter	**PBI**
E_a[kJ/mol]	16.2
τ_0 [s]	$1.75\ 10^{-9}$
M_2^{rigid} [G^2]	3.6
M_2^{motion} [G^2]	1.2

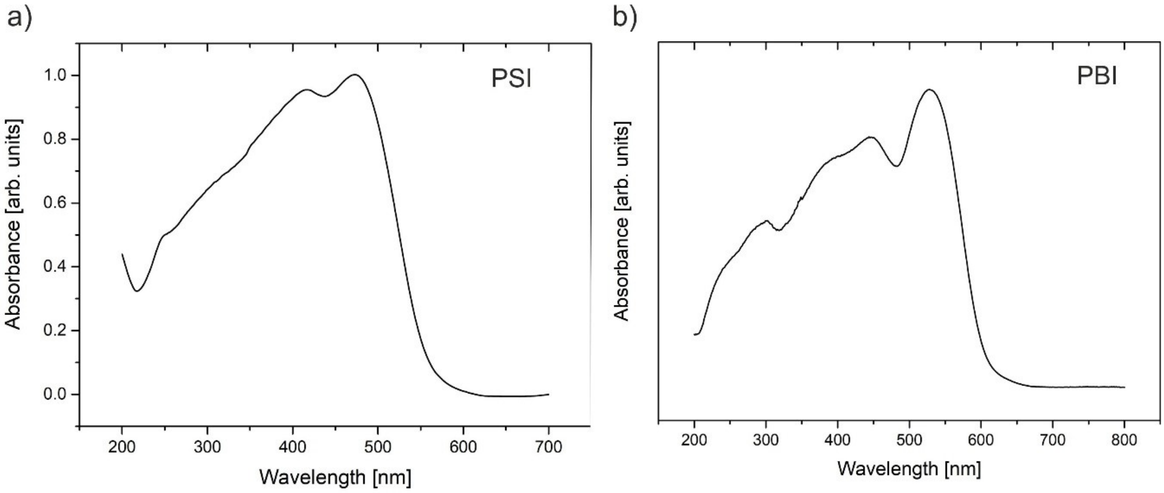

Fig. S6. Absorption spectrum UV-Vis for **PSI** and **PBI**.

References

1 CrysAlis PRO. Rigaku Corporation, Tokyo, Japan.
2 G. M. Sheldrick, *Acta Cryst.*, 2015, **C71**, 3.
3 P. Blaha, K. Schwarz, P. Sorantin, S. B. Trickey, *Comput. Phys. Commun.*, 1990, **59**, 399.
4 J. P. Perdew, K. Burke, M. Ernzerhof, *Phys. Rev. Lett.*, 1996, **77**, 3865.
5 W. Setyawan, S. Curtarolo, *Comput. Mater. Sci.*, **49**, 299.
6 A. Kokalj, *Proc. Symp. Softw. Dev. Process Mater. Des.,* 2003, **28**, 155.
7 N. Bloembergen , E.M. Purcell , R.V. Poun, Phys. Rev., 1948 **73**, 679.
8 J. H. van Vleck, *Phys. Rev.*, 1948, **74**, 1168.